QCD corrections in Standard Model EFT fits to WZ and WW production

Julien Baglio,[1,*] Sally Dawson,[2,†] and Samuel Homiller[2,3,‡]

[1]*Institute for Theoretical Physics, University of Tübingen, Auf der Morgenstelle 14, 72076 Tübingen, Germany*

[2]*Department of Physics, Brookhaven National Laboratory, Upton, New York 11973, USA*

[3]*C. N. Yang Institute for Theoretical Physics, Stony Brook University, Stony Brook, New York 11794, USA*

(Received 2 October 2019; published 30 December 2019)

We investigate the role of anomalous gauge boson and fermion couplings in the production of WZ and W^+W^- pairs at the LHC to next-to-leading-order (NLO) QCD in the Standard Model effective field theory (SMEFT), including dimension-six operators. Our results are implemented in a publicly available version of the POWHEG-BOX. We combine our WZ results in the leptonic final state $e\nu\mu^+\mu^-$ with previous W^+W^- results to demonstrate the numerical effects of NLO QCD corrections on the limits on effective couplings derived from ATLAS and CMS 8 and 13 TeV differential measurements. Our study demonstrates the importance of including NLO QCD SMEFT corrections in the WZ analysis, while the effects on WW production are smaller. We also show that the $\mathcal{O}(1/\Lambda^4)$ contributions dominate the analysis, where Λ is the high-energy scale associated with the SMEFT.

DOI: 10.1103/PhysRevD.100.113010

I. INTRODUCTION

The properties of the Standard Model (SM) have been experimentally verified at the LHC at the $\mathcal{O}$ (10–20%) level in the Higgs sector [1] and there is no evidence for the existence of any new particles or interactions at the TeV scale yet. High-statistics measurements of gauge boson pair production allow for detailed comparisons with Standard Model predictions and can be used to quantify the restrictions on anomalous interactions. Gauge boson pair production is particularly sensitive to new three-gauge-boson interactions [2] or new fermion-boson interactions [3]. The current task is to make comparisons between theory and data at the few-percent level which requires not only high-luminosity LHC running, but also improved theoretical calculations.

The SM rates for both W^+W^- and WZ production are well known. QCD corrections to WZ production in the Standard Model have been computed to next-to-leading order (NLO) for on-shell production [4,5] and to next-to-next-to-leading order (NNLO) for both on- and off-shell production [6,7]. SM electroweak corrections to the WZ process [8–12] are also known at NLO and can have significant effects in the high-p_T regime. W^+W^- pair production is also under good theoretical control in the SM: NNLO QCD [13–15] and NLO electroweak [8,9,16] corrections are understood and change the distributions and rates significantly.

Gauge boson pair production can be put under the microscope using an effective Lagrangian,

$$\mathcal{L}_{\text{SMEFT}} = \mathcal{L}_{\text{SM}} + \sum_{i,n} \frac{C_i^{(n)}}{\Lambda^{n-4}} O_i^{(n)} + \cdots, \tag{1}$$

where the new physics is parametrized as an operator expansion in inverse powers of a high scale Λ and the assumption is made that there are no light degrees of freedom. The operators $O_i^{(n)}$ have mass dimension n, are invariant under $SU(3) \times SU(2) \times U(1)$ and L_{SM} contains the complete SM Lagrangian. The subscript SMEFT (SM effective field theory) indicates that the Higgs is taken to be part of an $SU(2)$ doublet. At dimension-six, there are 59 possible operators [17,18] when flavor effects are neglected. We compute the amplitudes for W^+W^- and WZ pair production including the dimension-six operators, and then consider results when the cross sections are consistently expanded to both $1/\Lambda^2$ and $1/\Lambda^4$.

The leptonic decay channel of W^+W^- pair production has been studied at NLO in the SMEFT in a previous work [19]. Here we extend those results to include the leptonic decays from WZ pair production at the LHC in the presence of anomalous three-gauge-boson and anomalous fermion-gauge-boson couplings. QCD effects can affect the dependence of the kinematic distributions on the coefficients

*julien.baglio@cern.ch
†dawson@bnl.gov
‡samuel.homiller@stonybrook.edu

of Eq. (1). We include anomalous three-gauge-boson couplings and anomalous fermion-gauge-boson couplings in the POWHEG-BOX to NLO QCD in the SMEFT approach [20–23] following previous implementations for the SMEFT three-gauge-boson couplings case [24,25]. This public tool can be found at http://powhegbox.mib.infn.it.

Limits on SMEFT coefficients have been obtained in global fits that include gauge boson pair production, Higgs measurements, electroweak precision measurements, and top-quark measurements [26–30]. The SMEFT effects are treated at tree level in these fits, while the SM results include all known higher-order SM predictions. Fits attempting to use full NLO electroweak SMEFT predictions quickly observe that the plethora of operators makes such fits problematic [31,32]. On the other hand, the inclusion of NLO QCD SMEFT effects is simpler, due to the smaller number of operators involved [19,33,34].

In Sec. II, we define our notation in terms of anomalous couplings and present some calculational details. Section III contains a sampling of kinematic distributions with benchmark values of the anomalous couplings and Sec. IV has the results of a numerical fit to W^+W^- and WZ data. The NLO SMEFT QCD corrections have a numerically significant effect on many of the results. We point out that fits to $\mathcal{O}(1/\Lambda^2)$ or to $\mathcal{O}(1/\Lambda^4)$ result in quite different limits on the SMEFT coefficients. We conclude in Sec. V. We also provide fits using W^+W^- data only in Appendix A, while a discussion about the truncation at order $\mathcal{O}(1/\Lambda^2)$ is provided in Appendix B.

II. BASICS

A. Effective gauge and fermion interactions

We begin by reviewing the most general CP- and Lorentz-invariant Lagrangian for anomalous W^+W^-Z and $W^+W^-\gamma$ couplings [2,35],

$$\mathcal{L}_V = -ig_{WWV}\left[g_1^V(W^+_{\mu\nu}W^{-\mu}V^\nu - W^-_{\mu\nu}W^{+\mu}V^\nu) + \kappa^V W^+_\mu W^-_\nu V^{\mu\nu} + \frac{\lambda^V}{M_W^2}W^+_{\rho\mu}W^{-\mu}{}_\nu V^{\nu\rho}\right], \tag{2}$$

with $V=\gamma, Z$, $g_{WW\gamma}=e$, and $g_{WWZ}=g\cos\theta_W$ ($s_W \equiv \sin\theta_W$, $c_W \equiv \cos\theta_W$). The anomalous couplings are defined as $g_1^V = 1+\delta g_1^V$, $\kappa^V = 1+\delta\kappa^V$, where in the SM $\delta g_1^V = \delta\kappa^V = \lambda^V = 0$ and gauge invariance implies $\delta g_1^\gamma = 0$.

The effective couplings of quarks to gauge fields are[1] [3,19,31,36],

$$\mathcal{L} \equiv g_Z Z_\mu[g_L^{Zq}+\delta g_L^{Zq}]\bar{q}_L\gamma_\mu q_L + g_Z Z_\mu[g_R^{Zq}+\delta g_R^{Zq}]\bar{q}_R\gamma_\mu q_R + \frac{g}{\sqrt{2}}\{W_\mu[(1+\delta g_L^W)\bar{u}_L\gamma_\mu d_L + \delta g_R^W \bar{u}_R\gamma_\mu d_R] + \text{H.c.}\}. \tag{3}$$

Here, $g_Z = e/(c_W s_W) = g/c_W$ and q is an up- or down-flavor quark. The SM quark interactions are

$$g_R^{Zq} = -s_W^2 Q_q \quad \text{and} \quad g_L^{Zq} = T_3^q - s_W^2 Q_q, \tag{4}$$

where $T_3^q = \pm\frac{1}{2}$ and Q_q is the electric charge.

$SU(2)$ invariance implies,

$$\delta g_L^W = \delta g_L^{Zu} - \delta g_L^{Zd}, \quad \delta g_1^Z = \delta\kappa^Z + \frac{s_W^2}{c_W^2}\delta\kappa^\gamma, \quad \lambda^\gamma = \lambda^Z. \tag{5}$$

This framework leads to seven unknown parameters, $\delta g_1^Z, \delta\kappa_Z, \lambda_Z, \delta g_L^{Zu}, \delta g_L^{Zd}, \delta g_R^{Zu}$ and δg_R^{Zd}, contributing to W^+W^- production. The anomalous right-handed couplings do not contribute to WZ production, hence reducing the number of unknown parameters to five. These parameters are $\mathcal{O}(1/\Lambda^2)$ in the SMEFT language. The conversion between the effective Lagrangians of Eqs. (2) and (3) and the dimension-six interactions in the Warsaw basis can be found in many places [3,19,37] and there is a one-to-one mapping between the two approaches.[2]

It is of interest to study the high-energy limits of the helicity amplitudes for W^+W^- and WZ scattering in order to understand generic features of our results. In the high-energy limit ($s \gg M_Z^2$), only the longitudinal (00) and transverse ($\pm\mp$) helicity amplitudes remain nonzero in the SM WZ amplitudes (where s is the partonic center-of-mass energy squared) [38],

$$A_{00}^{SM,W^+Z} \to -\frac{g^2}{2\sqrt{2}}\sin\theta, \quad A_{\pm,\mp}^{SM,W^+Z} \to \frac{g^2}{\sqrt{2}}c_W\left(\frac{1-\cos\theta}{\sin\theta}\right)\left[\cos\theta + \frac{1}{3}\tan^2\theta_W\right], \quad A_{\pm,\pm}^{SM,W^+Z} \to \mathcal{O}\left(\frac{M_Z^2}{s}\right), \tag{6}$$

where θ is the center-of-mass angle of the W boson with respect to the up-quark direction and $g_L^{Zu} - g_L^{Zd} = c_W^2$. The radiation zero in the high-energy $(\pm,\mp)$ amplitude at $\cos\theta_0 = (g_L^{Zu}+g_L^{Zd})/(g_L^{Zu}-g_L^{Zd})$ is clearly seen in Eq. (6).

The SMEFT contributions to W^+Z production that contribute interference effects with the SM in the high-energy limit are [28,38],

[1]We assume no new tensor structures and neglect Cabibbo-Kobayashi-Maskawa mixing and all flavor effects. We assume SM gauge couplings to leptons, since these couplings are highly restricted by LEP data. We further neglect possible anomalous right-handed W-quark couplings, since they are suppressed by small Yukawa couplings in a minimal-flavor-violation framework and stringently limited by Tevatron and LHC measurements.

[2]See for example, Tables 4 and 5 of Ref. [19].

$$\delta A_{00}^{W^+Z} \to \frac{g^2}{2\sqrt{2}}\sin\theta\left(\frac{s}{M_Z^2}\right)\left[\delta g_1^Z + \frac{(\delta g_L^{Zd} - \delta g_L^{Zu})}{c_W^2}\right],$$
$$\delta A_{\pm\pm}^{W^+Z} \to \frac{g^2}{2\sqrt{2}c_W}\sin\theta\left(\frac{s}{M_Z^2}\right)\lambda_Z,$$
$$\delta A_{\pm,\mp}^{W^+Z} \to -\frac{g^2}{\sqrt{2}c_W}\sin\theta\left[\delta g_L^{Zu}\tan^2\left(\frac{\theta}{2}\right) + \delta g_L^{Zd}\right]. \quad (7)$$

Note that in the high-energy limit, $s \gg M_Z^2$, the dependence on $\delta\kappa_Z$ is suppressed and that the energy-enhanced longitudinal amplitude peaks at $\theta = \frac{\pi}{2}$. Only the longitudinal modes have an energy-enhanced interference contribution with the SM. The approximate zero of the SM $(\pm\mp)$ amplitude is weakened in the high-energy limit where contributions from the anomalous fermion couplings fill in the dip at $\cos\theta_0$.

The complete helicity amplitudes for W^+W^- production can be found in Refs. [2,33]. The energy-enhanced amplitudes for $q_{L,R}\bar{q}_{L,R} \to W^+W^-$ are,

$$\delta A_{LL00}^{W^+W^-} = \frac{g^2}{2}\frac{s}{M_W^2}\sin\theta[\delta\kappa_Z(Q_q - T_3^q) - c_W^2 Q_q \delta g_1^Z - \delta g_L^{Zq} + 2T_3^q \delta g_L^W],$$
$$\delta A_{RR00}^{W^+W^-} = \frac{g^2}{2}\frac{s}{M_W^2}\sin\theta[-Q_q\delta\kappa_Z + c_W^2 Q_q \delta g_1^Z + \delta g_R^{Zq}]. \quad (8)$$

Due to the Goldstone boson nature of the longitudinal modes, the amplitudes of Eqs. (7) and (8) satisfy

$$\delta A_{00}^{W^+Z} = \delta A_{LL00}^{W^+W^-}(\bar{u}_L u_L \to W^+W^-) - \delta A_{LL00}^{W^+W^-}(\bar{d}_L d_L \to W^+W^-). \quad (9)$$

This implies that the high-energy limits of WV production $(V = W, Z)$ are only sensitive to four combinations of coefficients, and the dependence on other parameters is suppressed by powers of $\frac{M_W^2}{s}$ [28,39–41].

The amplitudes for W^+W^- and WZ production can be schematically written as,

$$A \sim A_{\rm SM} + \frac{\delta A_{\rm EFT}^{(6)}}{\Lambda^2} + \frac{\delta A_{\rm EFT}^{(8)}}{\Lambda^4} + \cdots \quad (10)$$

The cross section is then,

$$\sigma \sim \frac{1}{s}\left[|A_{\rm SM}|^2 + 2{\rm Re}\left(\frac{A_{\rm SM}^* \delta A_{\rm EFT}^{(6)}}{\Lambda^2}\right) + \frac{|\delta A_{\rm EFT}^{(6)}|^2}{\Lambda^4} + 2{\rm Re}\left(\frac{A_{\rm SM}^* \delta A_{\rm EFT}^{(8)}}{\Lambda^4}\right) + \cdots\right]. \quad (11)$$

In the results of this paper, we implicitly assume that the $1/\Lambda^4$ contributions from the dimension-eight operators can be neglected, so that terms of $\mathcal{O}(1/\Lambda^4)$ in the cross section can be kept in a consistent way. This is the case, for example, in strongly interacting models [42,43]. We present an analysis of the truncation at $\mathcal{O}(1/\Lambda^2)$ in Appendix B, to check whether or not the $\mathcal{O}(1/\Lambda^4)$ terms are important.

B. Primitive cross sections

We want to compute differential and total cross sections for the WZ scattering process at NLO QCD for arbitrary anomalous couplings with kinematic cuts mimicking the experimental analyses. The current calculation uses identical techniques as in Ref. [19]. The decomposition into primitive cross sections works at both leading order (LO) and NLO and there are 15 primitive cross sections for the WZ process and 35 for the W^+W^- process at $\mathcal{O}(\Lambda^{-4})$.

C. Calculational details

We have implemented the process $pp \to WZ \to (l^+l^-)(l'\bar{\nu}')$ into the POWHEG-BOX-v2 including anomalous fermion and gauge boson couplings. The existing implementation [24] does not allow for anomalous fermion couplings. Our new implementation allows the user to chose the order of the Λ^{-2n} expansion and to use either the effective Lagrangians described in this work or the Warsaw basis coefficients. Note that we assume different flavor leptonic decays. The results shown in the following sections use CTEQ14qed parton distribution functions and we fix the renormalization/factorization scales at $M_Z/2$.

III. NLO EFFECTS IN WZ DISTRIBUTIONS

We now present distributions for various kinematic variables at LO and NLO with different values of the anomalous couplings using the methods described in the previous section. In addition to the Standard Model, we present results for two benchmark points:

$$\begin{aligned}\text{Gauge (or 3GB):}\ & \delta g_1^Z = 0.016, \quad \lambda^Z = 0.0045, \\ & \delta\kappa^Z = 0.024, \quad \delta g_L^{Zu} = \delta g_L^{Zd} = 0; \\ \text{Fermion (or Ferm.):}\ & \delta g_1^Z = \lambda^Z = \delta\kappa^Z = 0, \\ & \delta g_L^{Zu} = -0.0024, \quad \delta g_L^{Zd} = 0.003.\end{aligned} \quad (12)$$

Both of these points are near the boundaries of the allowed regions from fits to W^+W^- and WZ production and serve to illustrate the effects of anomalous couplings on the NLO QCD corrections.

In Fig. 1, we show the distributions in bins of m_T^{WZ} and p_T^Z along with the corresponding ratios of the NLO and LO predictions using the cuts from Ref. [44], where

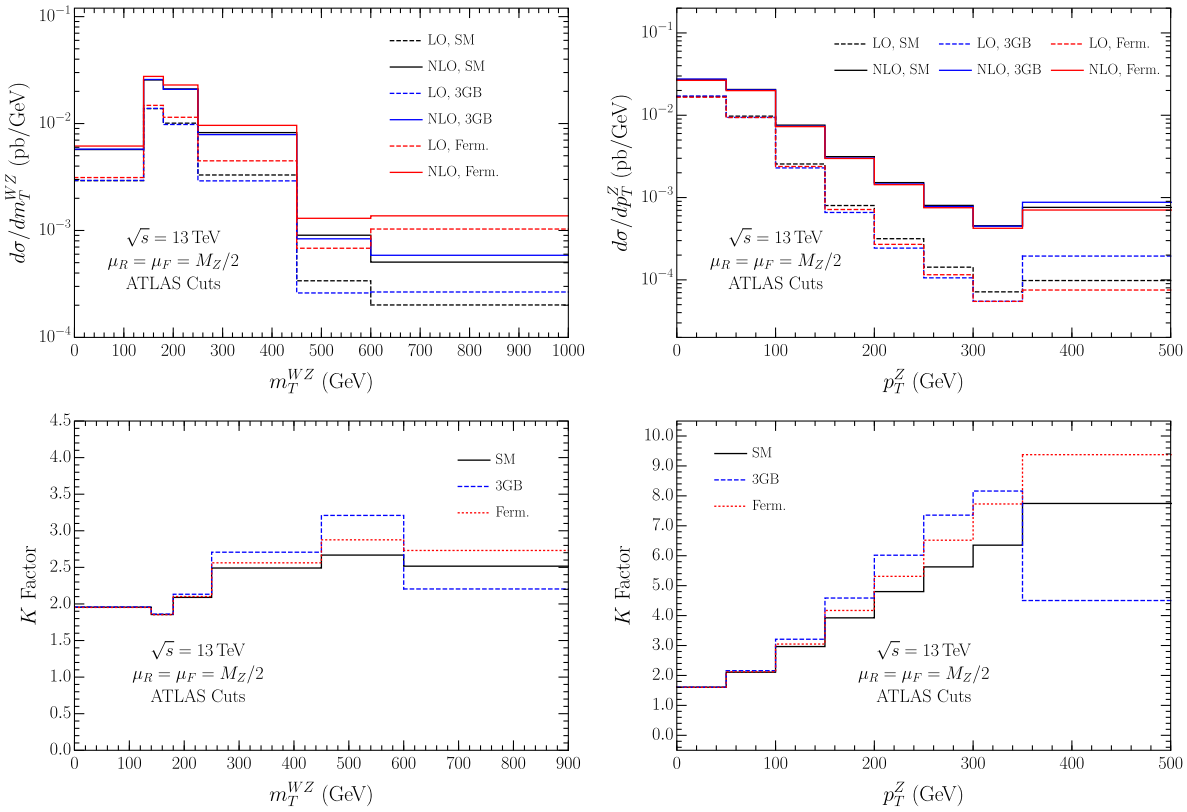

FIG. 1. Top row: Distributions at LO and NLO for the SM, anomalous gauge benchmark point and anomalous fermion benchmark point, Eq. (12), in bins of m_T^{WZ} and p_T^Z. Bottom row: K factors for the same three points. In both the m_T^{WZ} and p_T^Z distributions the final bin goes to 2 TeV.

$$m_T^{WZ} = \sqrt{\left(\sum_{\ell=1}^{3} p_T^\ell + E_T^{\rm miss}\right)^2 - \left(\sum_{\ell=1}^{3} p_x^\ell + E_x^{\rm miss}\right)^2 - \left(\sum_{\ell=1}^{3} p_y^\ell + E_y^{\rm miss}\right)^2}. \tag{13}$$

In the right panel we see that at high $p_{T,Z}$ the K factor[3] for the SM becomes very large as a result of real emission effects that arise at NLO, in agreement with Refs. [12,19]. In contrast, the K factor grows only modestly as a function of m_T^{WZ}. For the anomalous coupling benchmarks, we see that the K factor can change quite dramatically, particularly in the higher-momentum bins [22]. In the last p_T^Z bin in particular, the K factor changes from ∼7.8 in the SM to roughly 4.5 for our "Gauge" benchmark, and ∼9.4 for the "Fermion" point. Similar, but less dramatic, effects are seen in m_T^{WZ} as well.

The results of Fig. 1 clearly demonstrate that using the Standard Model K factor in an analysis of anomalous couplings in WZ production is inaccurate at large p_T^Z. As the high transverse momentum bins provide most of the constraining power for fits to the anomalous couplings, this can drastically change the resulting limits on the anomalous coefficients, as we demonstrate in the following sections.

We next consider the NLO effects on distributions of the angular variables $\cos\theta_W^*$ and ϕ_W^*. They are the angular variables of the decayed charged lepton in the W rest frame. We use the helicity coordinate system as defined by ATLAS [44], in which the z direction of the W rest frame is the W direction of flight as seen in the WZ center-of-mass frame. The definitions of the x and y axes are given in Ref. [45] and a graphical representation is given in Ref. [11] (with a slight modification for the z direction). Angular variables in the decay products (particularly $\cos\theta_W^*$) are useful for extracting maximal sensitivity to the gauge boson polarizations [46]. As emphasized in Refs. [40,41,46], SMEFT effects lead to quadratic energy growth at the interference level only in the amplitude for

[3]The K factor is defined as the ratio of the NLO/LO result for a given scenario.

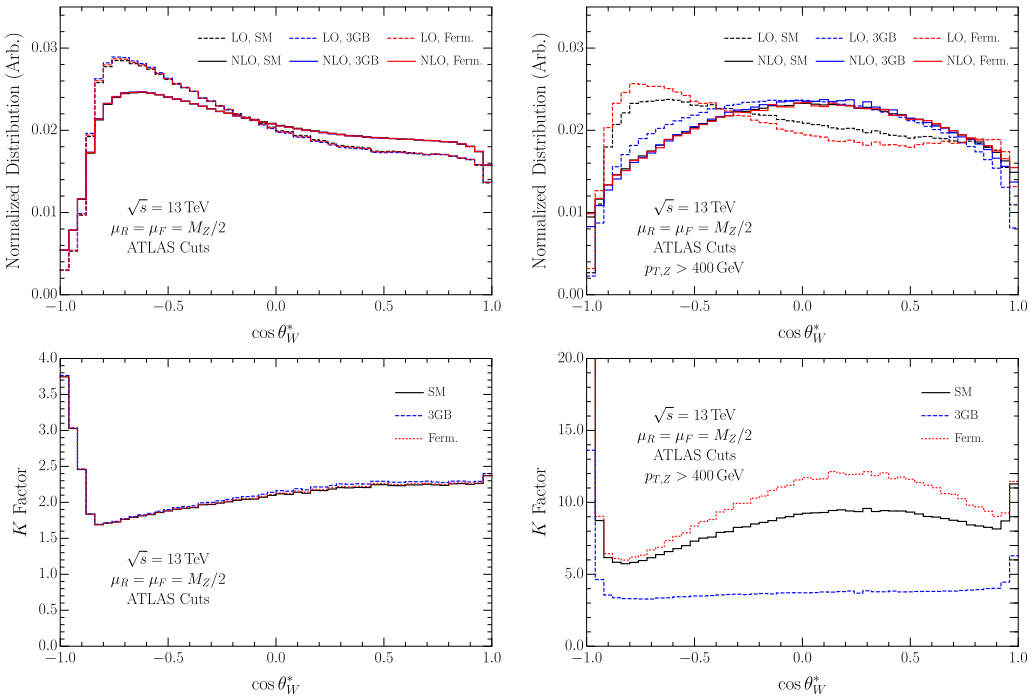

FIG. 2. Top row: Normalized distribution at LO and NLO for the SM, anomalous gauge interaction point and anomalous fermion benchmark points, Eq. (12), in bins of $\cos\theta^*_W$ with the ATLAS 13 TeV fiducial cuts [44]. The left panel shows the inclusive distribution, while the right panel shows the distribution after an additional cut requiring $p_{T,Z} > 400$ GeV. Bottom row: K factors for the same three points and for the same choice of cuts.

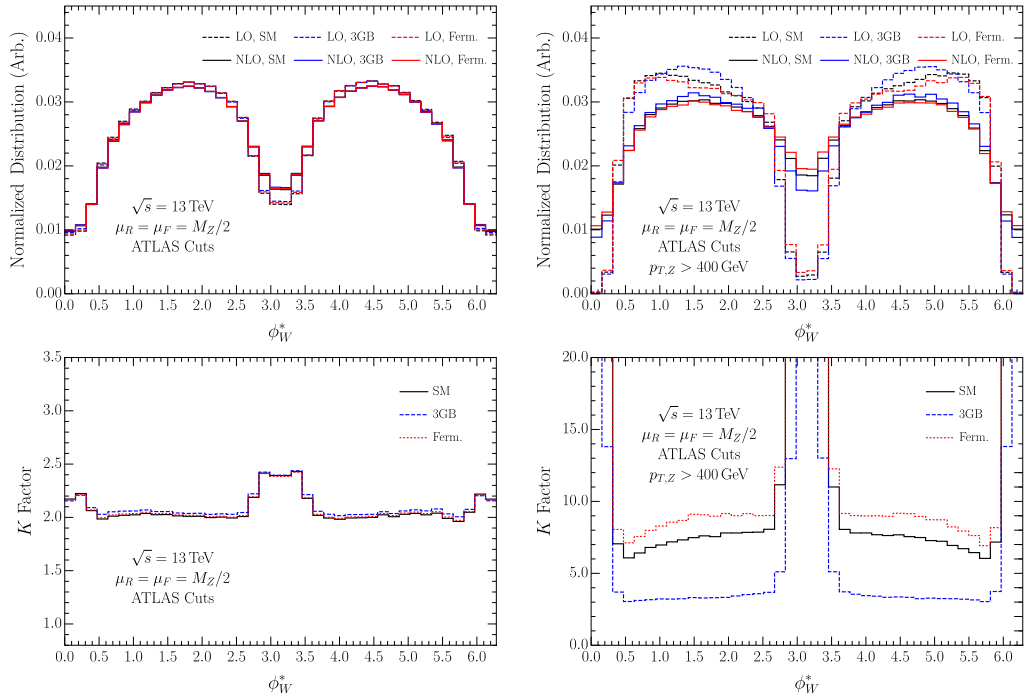

FIG. 3. The same as Fig. 2, but for the angular variable ϕ^*_W.

TABLE I. Experimental data included in our study. The third column shows the number of bins used in our analysis, always counting from the highest.

Channel	Distribution	# bins	Data set	Integrated luminosity
$WW \to \ell^+\ell'^- + \not{E}_T(0j)$	$p_T^{\text{leading lepton}}$, Fig. 11	1	ATLAS 8 TeV	20.3 fb^{-1} [48]
$WW \to e^\pm\mu^\mp + \not{E}_T(0j)$	$p_T^{\text{leading lepton}}$, Fig. 7	5	ATLAS 13 TeV	36.1 fb^{-1} [51]
$WZ \to \ell^+\ell^-\ell'^{(\prime)\pm}$	m_T^{WZ}, Fig. 5	2	ATLAS 8 TeV	20.3 fb^{-1} [52]
$WZ \to \ell^+\ell^-\ell'^{(\prime)\pm} + \not{E}_T$	Z candidate $p_T^{\ell\ell}$, Fig. 5	9	CMS 8 TeV	19.6 fb^{-1} [53]
$WZ \to \ell^+\ell^-\ell'^{(\prime)\pm}$	m_T^{WZ} Fig. 4c	6	ATLAS 13 TeV	36.1 fb^{-1} [44]
$WZ \to \ell^+\ell^-\ell'^{(\prime)\pm} + \not{E}_T$	m^{WZ}, Fig. 15a	3	CMS 13 TeV,	35.9 fb^{-1} [54]

producing two longitudinally polarized gauge bosons, Eq. (7). This behavior was exploited in Ref. [41] to maximize the sensitivity of the $p_{T,V}$ distribution to anomalous couplings.

In Figs. 2 and 3 we show the normalized distributions of $\cos\theta_W^*$ and ϕ_W^* for the SM and for our two benchmark points at the fiducial level (left) and with an additional cut requiring $p_{T,Z} > 400$ GeV (right) to enhance the sensitivity of the distributions to the anomalous couplings. Without the additional $p_{T,Z}$ cut, the distributions are quite insensitive to the small values of the anomalous couplings at our benchmark points. An interesting effect of the NLO corrections is the washing out of the radiation zero present at LO at $\cos\theta_W^* = -1$, evidenced by the large K factor in this part of phase space.

After including the $p_{T,Z}$ cut, the LO samples are enriched with longitudinally polarized gauge bosons, and the distributions become much more sensitive to the anomalous couplings. At NLO however, a great deal of this dependence is washed out as a result of the high-p_T bins being more densely populated due to the real emission present at this order [41,47]. While Ref. [41] suggested this could be ameliorated with a jet veto, it was also demonstrated in Ref. [47] that a hard jet in the process is required to maintain access to the interference terms which grow quadratically with energy and are most sensitive to the SMEFT effects.

IV. FITS

The results of Sec. III demonstrate that including higher-order QCD effects in WZ production in the presence of anomalous gauge and fermion couplings can lead to significantly different predictions than using the LO SMEFT calculation with the Standard Model K factor. We now consider how these effects change the observed limits on the anomalous couplings based on a fit to experimental data. We consider the results in the case of a fit to only WZ data, and then, as a step towards a global analysis, fit both W^+W^- and WZ data.

The existing experimental results on W^+W^- and WZ production at both 8 and 13 TeV are summarized in Table I. The W^+W^- data from ATLAS collected at 8 TeV in Ref. [48] is systematically lower than the SM prediction in the lower bins, particularly in the 250–350 GeV bin. We thus use only the highest bin in p_T^{lead} for our analysis. The W^+W^- data from CMS at 8 TeV in Ref. [49] includes both same- and different-flavor final states so there is a contribution from ZZ production that we have not computed, so we do not include this result. The ATLAS 13 TeV result with 3.16 fb^{-1} in Ref. [50] uses data that is also included in the updated result with 36.1 fb^{-1} [51], so we will exclude this result as well.

To perform the fits, we construct a χ^2 function with the data from the remaining six data sets from Refs. [44,51–54], using the distributions indicated in Table I. The data in the distributions for Refs. [44,51–53], including both statistical and systematic uncertainties was obtained from the corresponding supplementary information. We combine the different sources of uncertainty in quadrature in each bin, neglecting any correlations. The data in Refs. [48,54] is not available online, so we digitize the plots to obtain the observed data and statistical uncertainties and add an additional 5% systematic uncertainty bin by bin, again neglecting correlations. In each case, the Standard Model prediction for the W^+W^- or WZ contribution for each distribution was found by digitizing the plots in the experimental papers. To account for detector effects, we normalize our theory predictions bin by bin to agree with the Standard Model predictions taken from the experimental results.

A. Fits to WZ data

We first present the fits to the 8 and 13 TeV WZ data from ATLAS and CMS [44,52–54]. In Fig. 4 we show the 95% C.L. allowed regions from various two-parameter fits to the anomalous couplings, in each case fixing the other three couplings to zero. As anticipated in Sec. III, the constraints using the LO and NLO predictions for the SMEFT contributions are quite different. The constraints

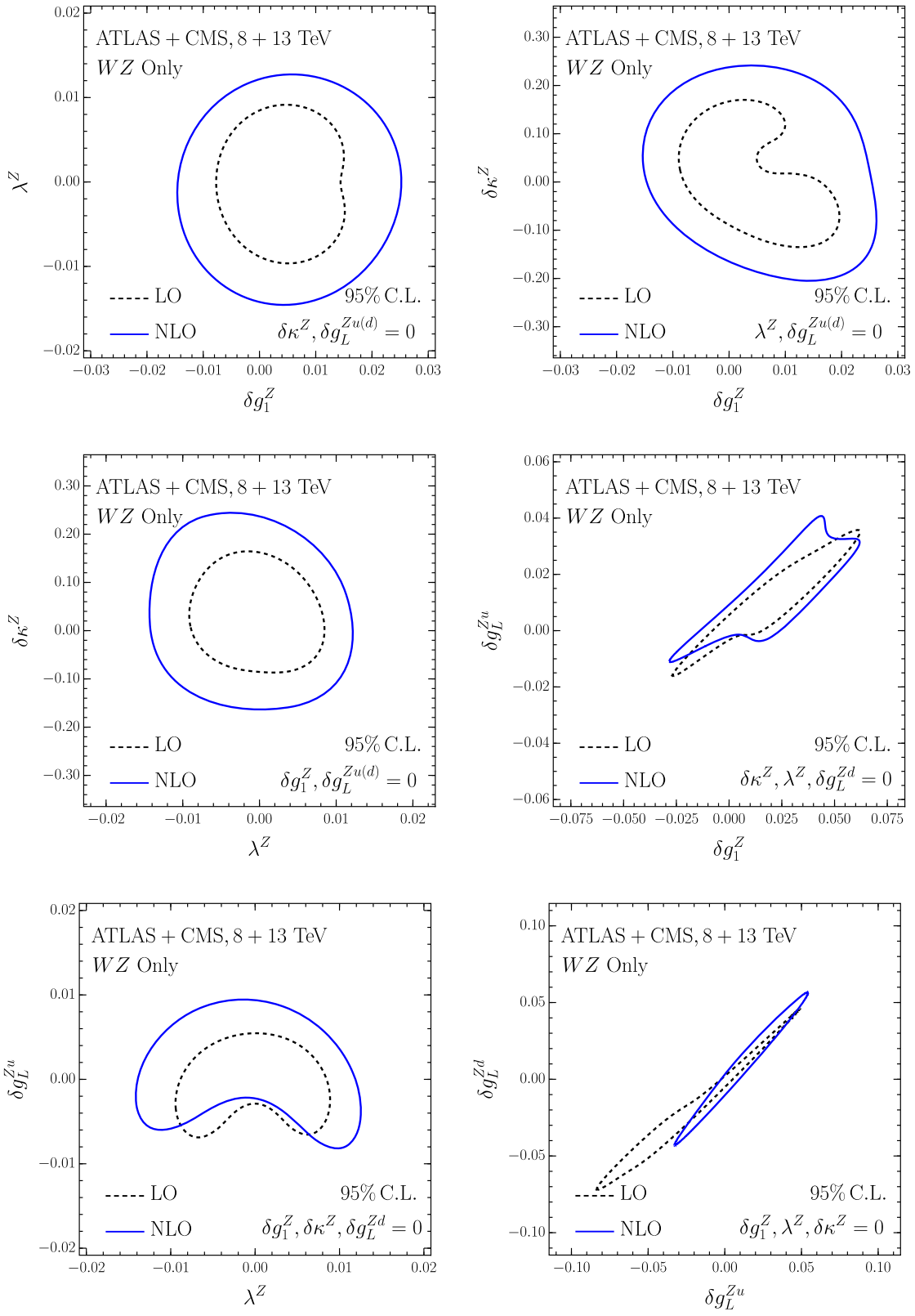

FIG. 4. 95% C.L. allowed regions for different combinations of anomalous gauge and fermion couplings based on a fit to the 8 and 13 TeV WZ data from ATLAS and CMS [44,52–54]. The results with the SMEFT treated at LO are shown as dashed black contours and the constraints with the SMEFT treated at NLO are shown in solid blue. In each panel we set the three couplings not shown to zero.

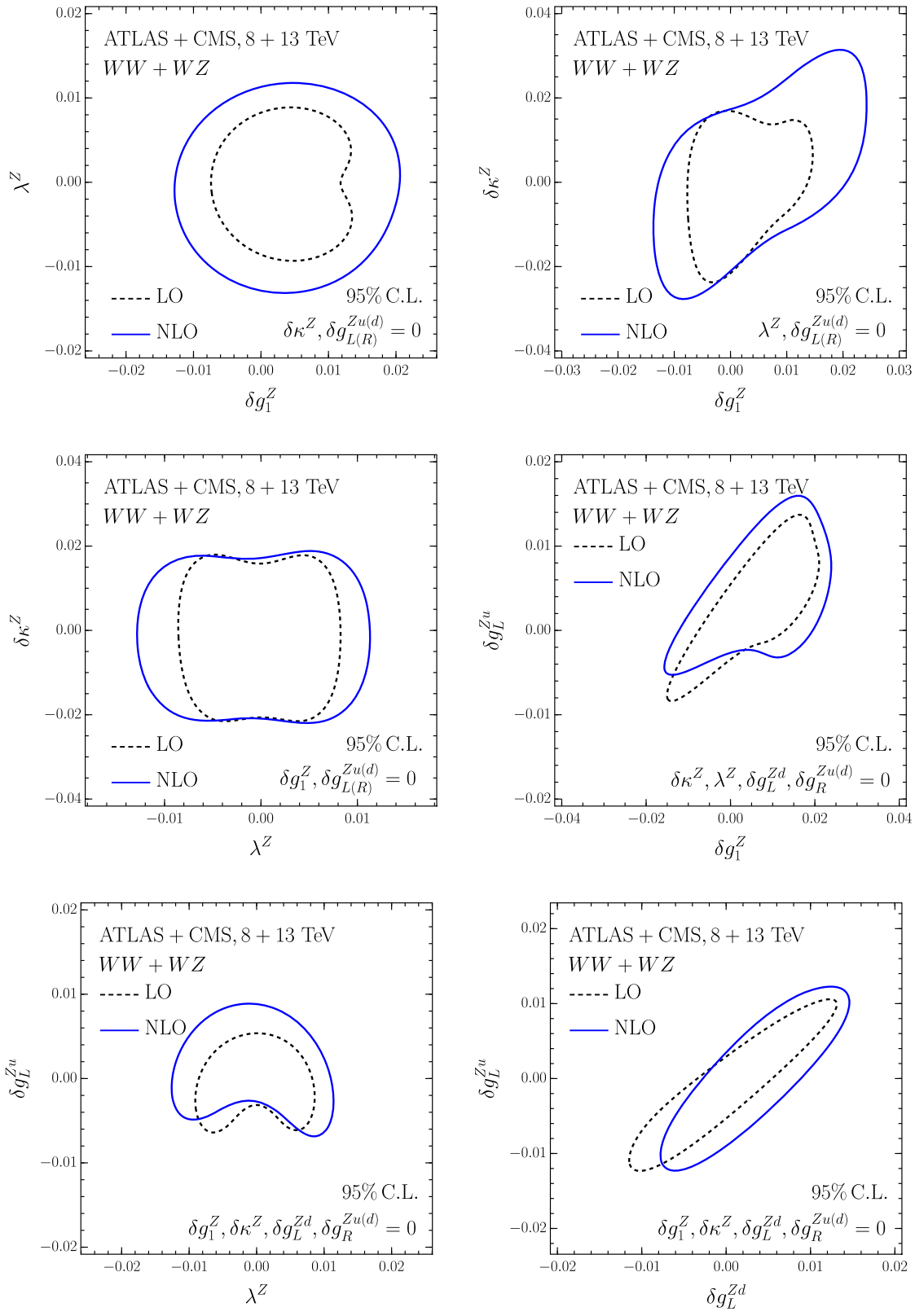

FIG. 5. As in Fig. 4, but using both WW and WZ data.

on the different combinations of gauge couplings are weaker, in some directions by a factor of 2. This is consistent with the behavior of the distributions with our "Gauge" benchmark point in Fig. 1. The effect is somewhat less dramatic in the case of anomalous fermion couplings, but there is still a large difference between the limits at LO and NLO.

In Sec. II A, we noted that the helicity amplitudes for WZ production had only a subleading (in s/M_Z^2) dependence on $\delta\kappa^Z$ in the high-energy limit. Measurements of WZ production are thus much less sensitive to $\delta\kappa^Z$, and we see in Fig. 4 that the limits on $\delta\kappa^Z$ are indeed an order of magnitude weaker than those on δg_1^Z and λ^Z. We also note that there is a near flat direction in the $\delta g_1^Z - \delta g_L^{Zu}$ plane, and an even more robust flat direction in the $\delta g_L^{Zu} - \delta g_L^{Zd}$ plane, in agreement with the scalings in Eq. (7).

B. Combined fits to W^+W^- and WZ data

In the previous section, it was demonstrated that treating the SMEFT consistently at NLO significantly changes the anomalous coupling constraints using WZ data only. On the other hand, in Ref. [19], it was shown that the NLO effects on W^+W^+ distributions in the presence of anomalous couplings are relatively mild; in other words, using the K factor derived at the SM is an adequate approximation for setting limits. It is of interest to understand to what extent the significant changes between LO and NLO fits in Fig. 4 remain when including W^+W^- data. Note that this is only a first step: the anomalous couplings are also constrained by other measurements both in Higgs data, top-quark physics and at LEP.

In Fig. 5, we consider the results for various combinations of couplings with the same setup as in Fig. 4, with the

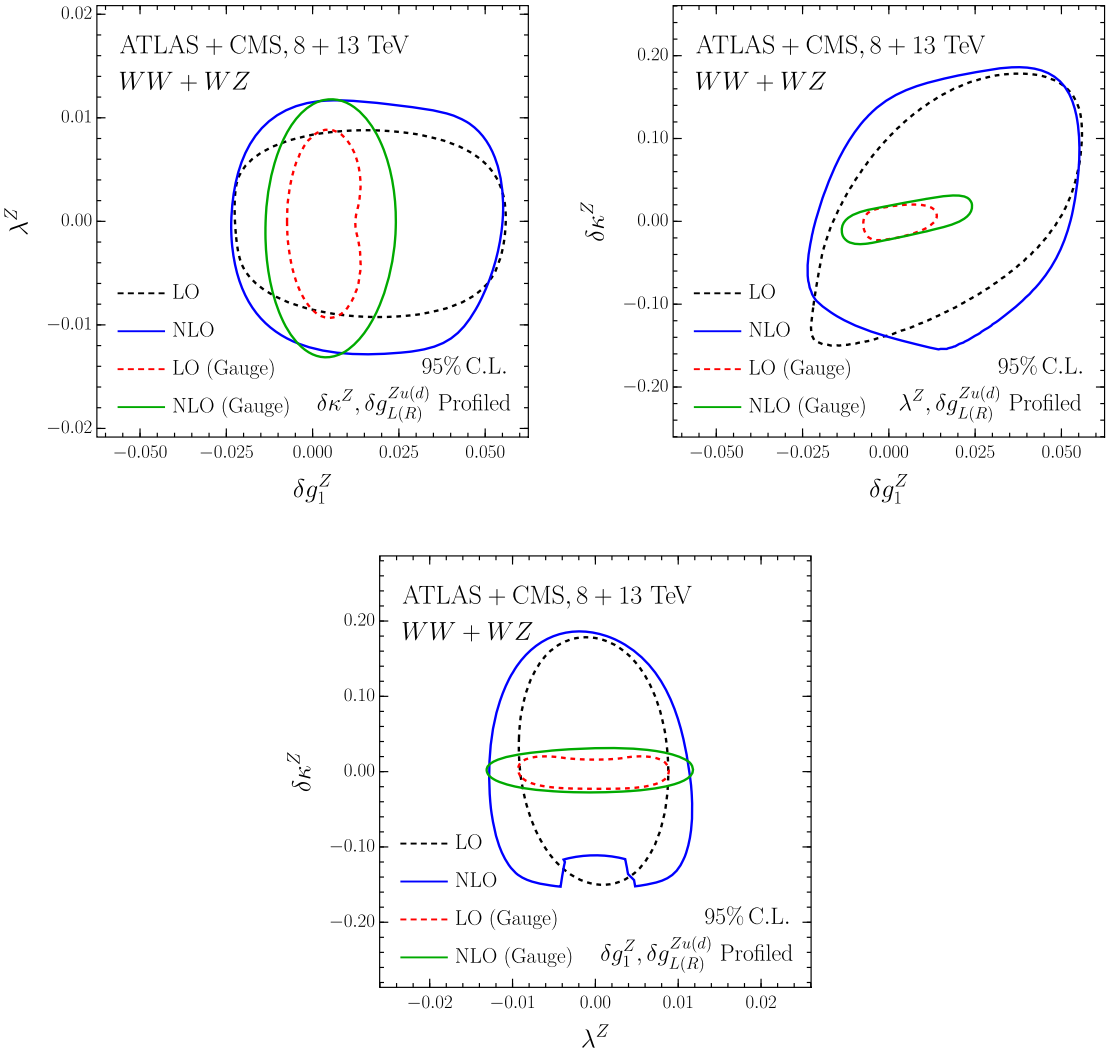

FIG. 6. As in Fig. 5, but profiling over the additional operators not shown. The red and green curves show the results profiling only over the gauge couplings at LO and NLO respectively.

other anomalous couplings fixed to zero. The most obvious result is that, even when combined with W^+W^- data, the effects of treating the SMEFT at NLO in WZ and W^+W^- production on the limits are still quite substantial in many directions in parameter space. The first panel is clearly mostly constrained by WZ data. As discussed in Sec. IV A, $\delta\kappa^Z$ is much better constrained when W^+W^- data is included, and since the NLO effects in W^+W^- production are very small, the limits in the $\delta\kappa^Z$-λ^Z plane (with all other couplings fixed to zero) are quite similar at LO and NLO. In the δg_1^Z-$\delta\kappa^Z$ plane, however, there is a flat direction in W^+W^- production in the high-energy limit [Eq. (8)], which is broken by the WZ data and the NLO effects are significant.

We have computed the rates up to quadratic order, $\mathcal{O}(1/\Lambda^4)$. This has a theoretical complication, however, because in principle dimension-eight operators may contribute at the same order in $1/\Lambda^4$ in the most general EFT framework and these effects are not considered here, as we have implicitly assumed that the contributions from the $\mathcal{O}(1/\Lambda^4)$ dimension-eight operators in the Lagrangian are subleading. We discuss the effects and inherent assumptions involved in truncating the SMEFT expansion explicitly at $\mathcal{O}(1/\Lambda^2)$, i.e., treating the anomalous couplings only to linear order, in Appendix B. This discussion shows that the $\mathcal{O}(1/\Lambda^4)$ terms in the cross section are the leading effect in our fits.

We consider the effects of marginalizing over the operators not shown in each plot. In practice, this is done by minimizing the χ^2 function at each point with respect to the other five couplings. In Fig. 6, we show the limits for the three combinations of anomalous gauge couplings, and compare the effects of profiling over the other five anomalous couplings in black (blue) for LO (NLO) with the results when profiling over only the last gauge coupling in red (green) for LO (NLO). In both cases, the effects of considering the anomalous couplings at NLO weaken the bounds on λ^Z. The limits on δg_1^Z in the δg_1^Z-$\delta\kappa^Z$ plane are also affected, though the effect is more prominent when profiling only over the gauge couplings. We also see the result, anticipated in Refs. [3,33,55], that the limits on the anomalous gauge couplings are generally much weaker when the fermion couplings are allowed to float within their

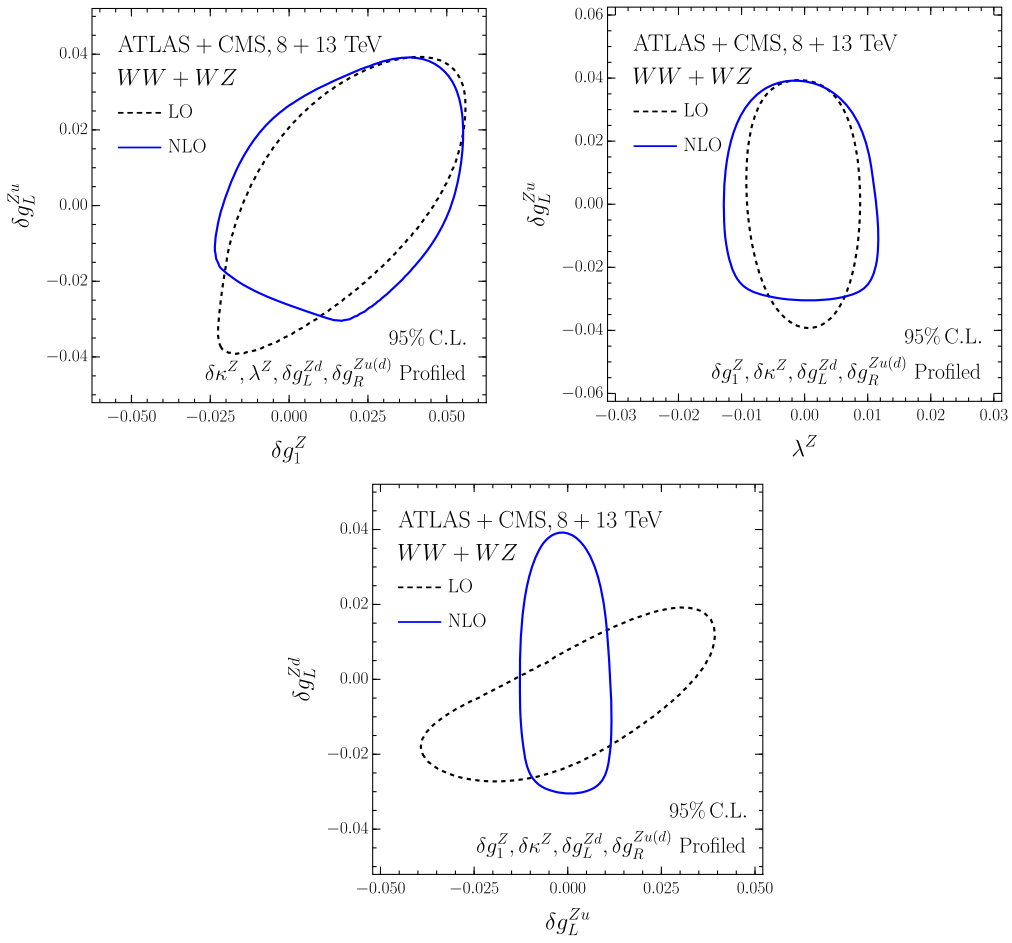

FIG. 7. As in Fig. 5, but profiling over the additional operators not shown.

TABLE II. 95% C.L. limits on the individual anomalous couplings based on a fit to W^+W^- and WZ data at LO and NLO, projecting out or profiling over the other couplings.

	LO allowed range		NLO allowed range	
Coupling	Projected	Profiled	Projected	Profiled
δg_1^Z	$[-0.007, 0.005]$	$[-0.015, 0.048]$	$[-0.012, 0.018]$	$[-0.016, 0.049]$
λ^Z	$[-0.008, 0.008]$	$[-0.009, 0.008]$	$[-0.012, 0.010]$	$[-0.012, 0.011]$
$\delta\kappa^Z$	$[-0.020, 0.015]$	$[-0.135, 0.158]$	$[-0.020, 0.017]$	$[-0.115, 0.168]$
δg_L^{Zu}	$[-0.002, 0.005]$	$[-0.034, 0.034]$	$[-0.001, 0.008]$	$[-0.022, 0.035]$
δg_R^{Zu}	$[-0.012, 0.014]$	$[-0.084, 0.086]$	$[-0.012, 0.014]$	$[-0.083, 0.096]$
δg_L^{Zd}	$[-0.005, 0.002]$	$[-0.025, 0.014]$	$[-0.008, 0.002]$	$[-0.025, 0.023]$
δg_R^{Zd}	$[-0.018, 0.017]$	$[-0.045, 0.048]$	$[-0.018, 0.017]$	$[-0.053, 0.043]$

allowed regions. This is only not true in the λ^Z direction, as the introduction of λ^Z leads to a fundamentally different scaling at high energies for the production of transversely polarized WZ [see Eq. (7)].

In Fig. 7, we show the constraints in various planes including anomalous fermion couplings, profiling over all five additional parameters. The NLO effects are again apparent, particularly in removing the remaining correlation between δg_L^{Zu} and δg_L^{Zd}. Finally, we summarize our results in the form of one-parameter limits on each of the anomalous couplings considered in Table II.

C. Validity of our results

The EFT Lagrangian of Eq. (1) is an expansion in powers of $(\text{Energy})^2/\Lambda^2$ and so is only valid for energies less than

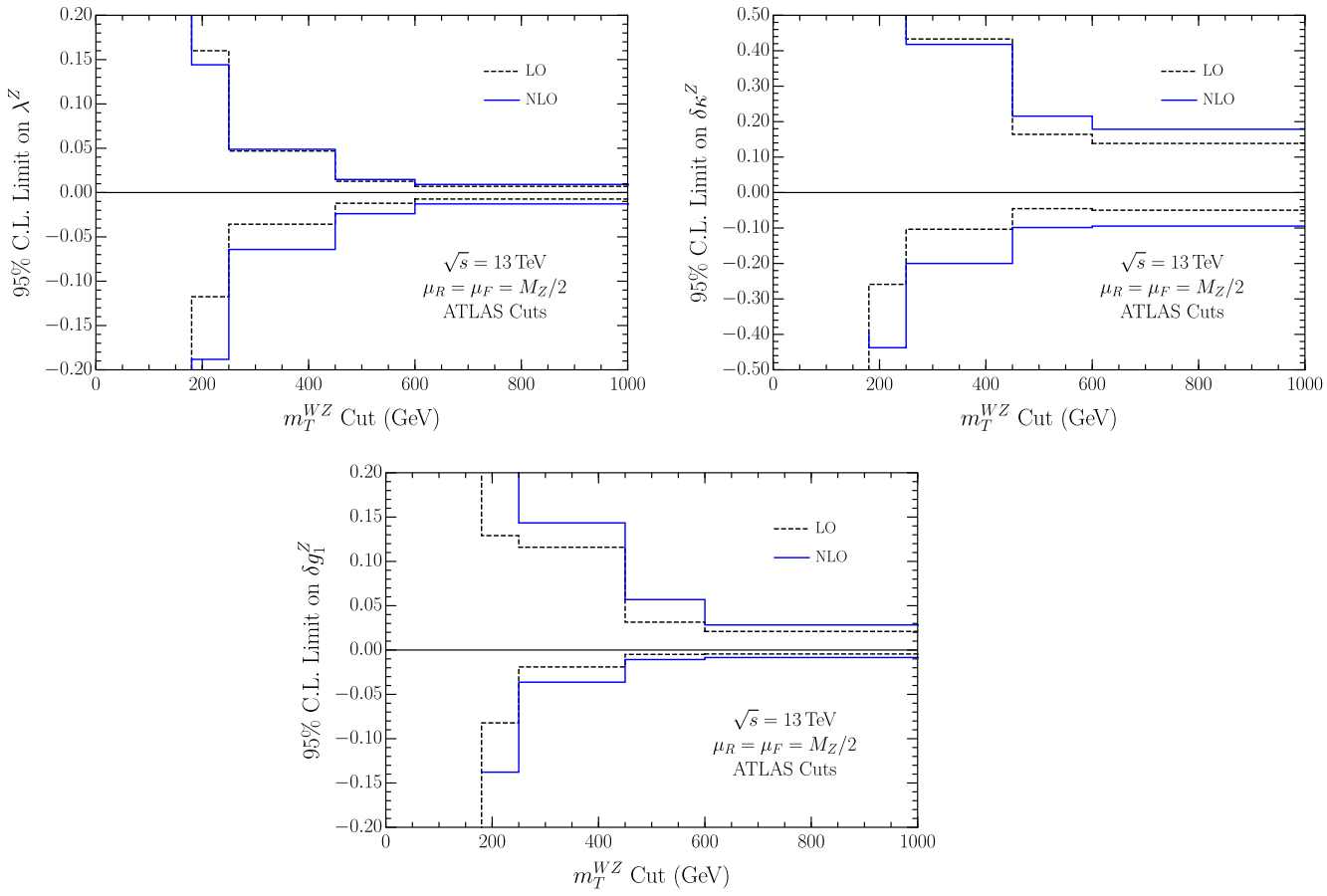

FIG. 8. Single-parameter fits to ATLAS 13 TeV WZ data, when successively removing the high-m_T^{WZ} bins.

the scale Λ [43,56]. We consider in Fig. 8 the effects of successively removing the high-energy bins from the single-parameter fits to the ATLAS 13 TeV WZ data. If we remove the top bin from the fit, $m_T^{WZ} > 600$ GeV, then all points in this fit satisfy $m_T^{WZ} < \Lambda$ (with $\Lambda = 1$ TeV) and the EFT is clearly a valid expansion. In this case, the fit is degraded by $\mathcal{O}(10\%)$ on $\delta\kappa^Z$ and $\mathcal{O}(30\%)$ for λ^Z and δg_1^Z, and the NLO QCD effects remain important. It would be interesting to have experimental results where the overflow bin is explicitly separated, so that the maximum energy of the data points in the last bin is clear. The result that interesting limits can be obtained even disregarding the highest-energy bin has been demonstrated using machine learning for the case of WH production in Ref. [57].

V. CONCLUSIONS

The SMEFT NLO QCD calculation for $pp \to WZ \to (l'\nu')(l^+l^-)$ has been included in the POWHEG-BOX and the primitive cross sections needed to reproduce our results at 8 and 13 TeV can be found at https://quark.phy.bnl.gov/Digital_Data_Archive/dawson/wz_19. The NLO QCD effects are significant for WZ production and have an important effect on the global fits to anomalous couplings. The $\mathcal{O}(1/\Lambda^4)$ terms dominate over the $\mathcal{O}(1/\Lambda^2)$ terms also when NLO QCD corrections are taken into account. We emphasize again that these results should be interpreted as only a first step in a profiled, global analysis, as all of the couplings—especially the fermionic ones—will be further constrained, and some flat directions removed, by data from LEP and Higgs measurements.

ACKNOWLEDGMENTS

We thank Anke Biekötter and Tilman Plehn for useful discussions of the global fits and Ian Lewis for insights into gauge boson pair production. S. D. is supported by the United States Department of Energy under Grant Contract No. DE-SC0012704 and is grateful to the University of Tübingen, where this work was started. The work of S. H. was supported in part by the National Science Foundation Grant No. PHY-1620628 and in part by Grant No. PHY-1915093. S. H. was also supported by the U.S. Department of Energy, Office of Science, Office of Workforce Development for Teachers and Scientists, Office of Science Graduate Student Research (SCGSR) program. The SCGSR program is administered by the Oak Ridge Institute for Science and Education (ORISE) for the DOE. ORISE is managed by ORAU under Contract No. DE-SC0014664. J. B. acknowledges the support from the Carl-Zeiss foundation. Parts of this work were performed thanks to the support of the State of Baden Württemberg through bwHPC and the DFG through the Grant No. INST 39/963-1 FUGG.

APPENDIX A: FITS TO W^+W^- PRODUCTION

In this appendix we present constraints on the anomalous gauge and fermion couplings based on only the W^+W^- data from ATLAS detailed in Table I. In Fig. 9, we show the two-dimensional limits setting the other anomalous couplings to zero. It is apparent that the NLO QCD effects do not have a significant impact on fits to the W^+W^- data alone.

APPENDIX B: TRUNCATION TO $1/\Lambda^2$

If the anomalous couplings are assumed to be small, then the dominant contribution is from the $\mathcal{O}(1/\Lambda^2)$ terms which are linear in the anomalous couplings. The results of such a linearized fit are shown in Fig. 10. Since this fit does not include the full amplitude squared, but just the interference terms it is not guaranteed to be positive definite. The regions with negative cross sections are shaded in grey (blue) for the LO (NLO) predictions, corresponding to regions where the linear approximation is not valid. A comparison of the linear and quadratic fits of Fig. 10 demonstrates that the fits are dominated by the quadratic $\mathcal{O}(1/\Lambda^4)$ contributions, and hence the data is not yet sensitive to weak anomalous couplings where the linear approximation would be valid.

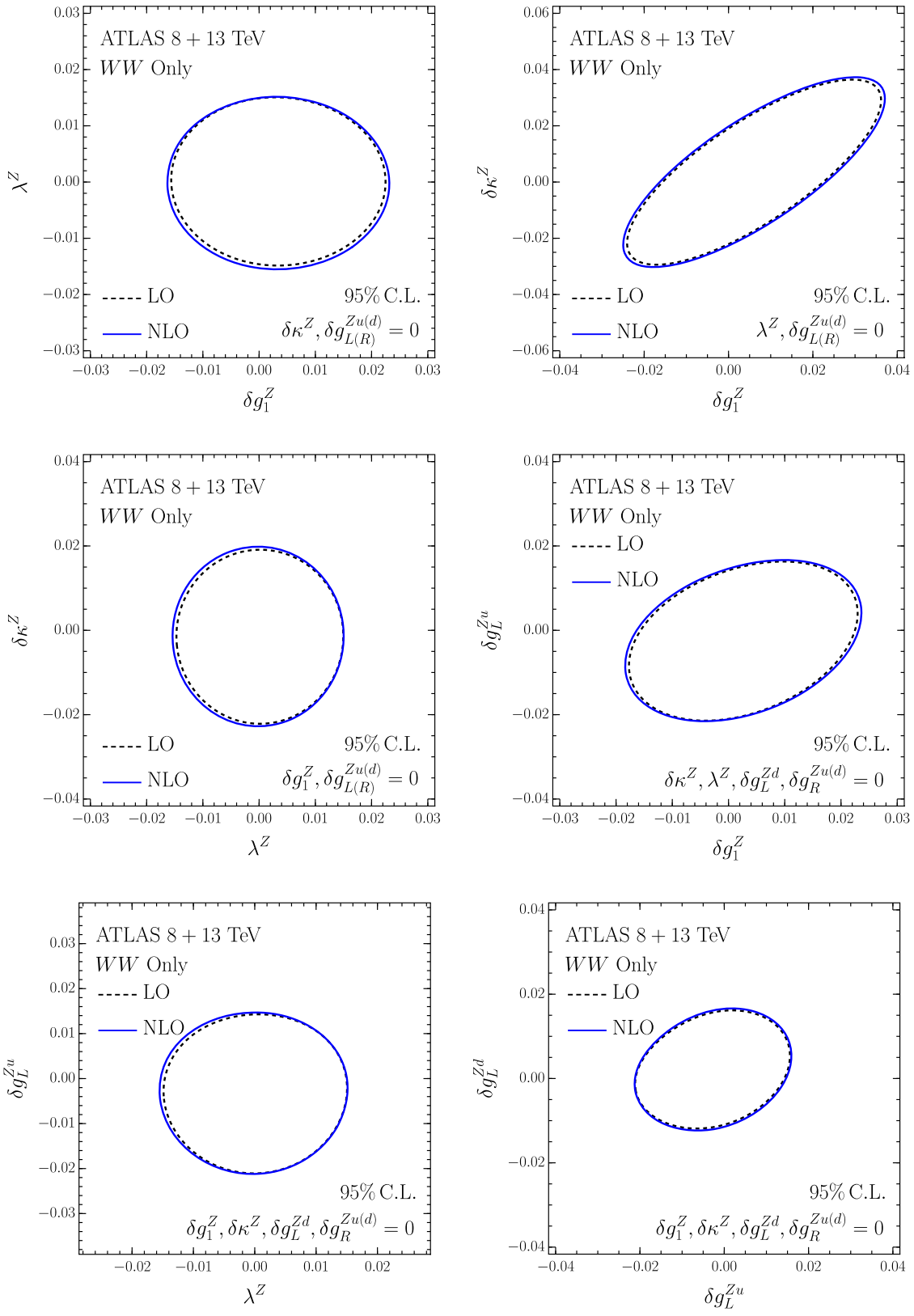

FIG. 9. As in Fig. 4, but using only *WW* data.

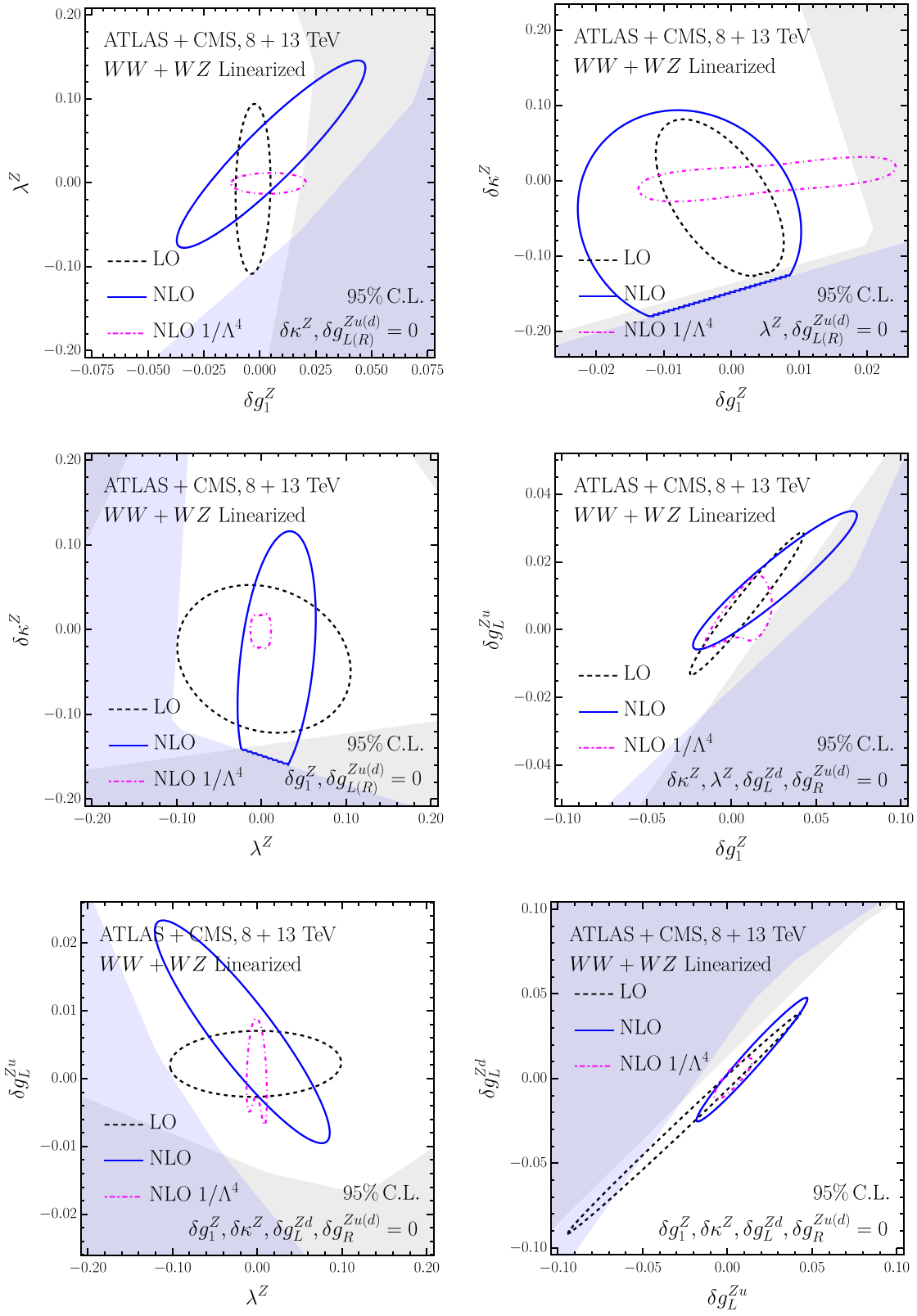

FIG. 10. The same as Fig. 5, but keeping only the leading terms in $1/\Lambda^2$. Regions where the predicted cross section in any of the bins used for the fit becomes negative are shown in grey (blue for NLO). We include the $1/\Lambda^4$ NLO results (pink) for comparison.

[1] S. Dawson, C. Englert, and T. Plehn, Higgs Physics: It ain't over till it's over, Phys. Rep. **816**, 1 (2019).

[2] K. Hagiwara, R. D. Peccei, D. Zeppenfeld, and K. Hikasa, Probing the weak Boson sector in $e^+e^- \to W^+W^-$, Nucl. Phys. **B282**, 253 (1987).

[3] Z. Zhang, Time to Go Beyond Triple-Gauge-Boson-Coupling Interpretation of W Pair Production, Phys. Rev. Lett. **118**, 011803 (2017).

[4] J. Ohnemus, Order-α_s calculation of hadronic $w^{\pm}$z production, Phys. Rev. D **44**, 3477 (1991).

[5] S. Frixione, P. Nason, and G. Ridolfi, Strong corrections to W Z production at hadron colliders, Nucl. Phys. **B383**, 3 (1992).

[6] M. Grazzini, S. Kallweit, D. Rathlev, and M. Wiesemann, $W^{\pm}Z$ production at hadron colliders in NNLO QCD, Phys. Lett. B **761**, 179 (2016).

[7] M. Grazzini, S. Kallweit, D. Rathlev, and M. Wiesemann, $W^{\pm}Z$ production at the LHC: Fiducial cross sections and distributions in NNLO QCD, J. High Energy Phys. 05 (2017) 139.

[8] A. Bierweiler, T. Kasprzik, and J. H. Kuhn, Vector-boson pair production at the LHC to $\mathcal{O}(\alpha^3)$ accuracy, J. High Energy Phys. 12 (2013) 071.

[9] J. Baglio, L. D. Ninh, and M. M. Weber, Massive gauge boson pair production at the LHC: A next-to-leading order story, Phys. Rev. D **88**, 113005 (2013); **94**, 099902(E) (2016).

[10] B. Biedermann, A. Denner, and L. Hofer, Next-to-leading-order electroweak corrections to the production of three charged leptons plus missing energy at the LHC, J. High Energy Phys. 10 (2017) 043.

[11] J. Baglio and N. Le Duc, Fiducial polarization observables in hadronic WZ production: A next-to-leading order QCD + EW study, J. High Energy Phys. 04 (2019) 065.

[12] A. Denner, S. Dittmaier, P. Maierhofer, M. Pellen, and C. Schwan, QCD and electroweak corrections to WZ scattering at the LHC, J. High Energy Phys. 06 (2019) 067.

[13] T. Gehrmann, M. Grazzini, S. Kallweit, P. Maierhofer, A. von Manteuffel, S. Pozzorini, D. Rathlev, and L. Tancredi, W^+W^- Production at Hadron Colliders in Next to Next to Leading Order QCD, Phys. Rev. Lett. **113**, 212001 (2014).

[14] F. Caola, K. Melnikov, R. Rontsch, and L. Tancredi, QCD corrections to W^+W^- production through gluon fusion, Phys. Lett. B **754**, 275 (2016).

[15] M. Grazzini, S. Kallweit, S. Pozzorini, D. Rathlev, and M. Wiesemann, W^+W^- production at the LHC: Fiducial cross sections and distributions in NNLO QCD, J. High Energy Phys. 08 (2016) 140.

[16] B. Biedermann, M. Billoni, A. Denner, S. Dittmaier, L. Hofer, B. Jäger, and L. Salfelder, Next-to-leading-order electroweak corrections to $pp \to W^+W^- \to 4$ leptons at the LHC, J. High Energy Phys. 06 (2016) 065.

[17] W. Buchmuller and D. Wyler, Effective Lagrangian qnalysis of new interactions and flavor conservation, Nucl. Phys. **B268**, 621 (1986).

[18] B. Grzadkowski, M. Iskrzynski, M. Misiak, and J. Rosiek, Dimension-six terms in the Standard Model Lagrangian, J. High Energy Phys. 10 (**2010**) 085.

[19] J. Baglio, S. Dawson, and I. M. Lewis, NLO effects in EFT fits to W^+W^- production at the LHC, Phys. Rev. D **99**, 035029 (2019).

[20] L. J. Dixon, Z. Kunszt, and A. Signer, Helicity amplitudes for O(alpha-s) production of W^+W^-, $W^{\pm}Z$, ZZ, $W^{\pm}\gamma$, or $Z\gamma$ pairs at hadron colliders, Nucl. Phys. **B531**, 3 (1998).

[21] L. J. Dixon, Z. Kunszt, and A. Signer, Vector boson pair production in hadronic collisions at order α_s: Lepton correlations and anomalous couplings, Phys. Rev. D **60**, 114037 (1999).

[22] U. Baur, T. Han, and J. Ohnemus, WZ production at hadron colliders: Effects of nonstandard WWZ couplings and QCD corrections, Phys. Rev. D **51**, 3381 (1995).

[23] A. Azatov, D. Barducci, and E. Venturini, Precision diboson measurements at hadron colliders, J. High Energy Phys. 04 (2019) 075.

[24] T. Melia, P. Nason, R. Rontsch, and G. Zanderighi, W+W-, WZ and ZZ production in the POWHEG BOX, J. High Energy Phys. 11 (2011) 078.

[25] P. Nason and G. Zanderighi, W^+W^-, WZ and ZZ production in the POWHEG-BOX-V2, Eur. Phys. J. C **74**, 2702 (2014).

[26] J. de Blas, M. Ciuchini, E. Franco, S. Mishima, M. Pierini, L. Reina, and L. Silvestrini, The Global electroweak and Higgs fits in the LHC era, Proc. Sci., EPS-HEP2017 (**2017**) 467 [arXiv:1710.05402].

[27] J. Ellis, C. W. Murphy, V. Sanz, and T. You, Updated Global SMEFT fit to Higgs, Diboson and electroweak data, J. High Energy Phys. 06 (2018) 146.

[28] C. Grojean, M. Montull, and M. Riembau, Diboson at the LHC vs LEP, J. High Energy Phys. 03 (2019) 020.

[29] E. da Silva Almeida, A. Alves, N. Rosa Agostinho, O. J. P. Éboli, and M. C. Gonzalez-Garcia, Electroweak sector under scrutiny: A combined analysis of LHC and electroweak precision data, Phys. Rev. D **99**, 033001 (2019).

[30] A. Biekotter, T. Corbett, and T. Plehn, The Gauge-Higgs legacy of the LHC Run II, SciPost Phys. **6**, 064 (2019).

[31] L. Berthier, M. Bjorn, and M. Trott, Incorporating doubly resonant $W^{\pm}$ data in a global fit of SMEFT parameters to lift flat directions, J. High Energy Phys. 09 (2016) 157.

[32] S. Dawson and P. P. Giardino, Electroweak and QCD Corrections to Z and W pole observables in the SMEFT, arXiv:1909.02000.

[33] J. Baglio, S. Dawson, and I. M. Lewis, An NLO QCD effective field theory analysis of W^+W^- production at the LHC including fermionic operators, Phys. Rev. D **96**, 073003 (2017).

[34] N. P. Hartland, F. Maltoni, E. R. Nocera, J. Rojo, E. Slade, E. Vryonidou, and C. Zhang, A Monte Carlo global analysis of the Standard Model effective field theory: The top quark sector, J. High Energy Phys. 04 (2019) 100.

[35] K. J. F. Gaemers and G. J. Gounaris, Polarization amplitudes for $e^+e^- \to W^+W^-$ and $e^+e^- \to ZZ$, Z. Phys. C **1**, 259 (1979).

[36] A. Falkowski and F. Riva, Model-independent precision constraints on dimension-6 operators, J. High Energy Phys. 02 (2015) 039.

[37] L. Berthier and M. Trott, Towards consistent electroweak precision data constraints in the SMEFT, J. High Energy Phys. 05 (2015) 024.

[38] U. Baur, T. Han, and J. Ohnemus, Amplitude Zeros in $W^{\pm}Z$ Production, Phys. Rev. Lett. **72**, 3941 (1994).

[39] R. S. Gupta, A. Pomarol, and F. Riva, BSM Primary Effects, Phys. Rev. D **91**, 035001 (2015).
[40] A. Falkowski, M. Gonzalez-Alonso, A. Greljo, D. Marzocca, and M. Son, Anomalous triple gauge couplings in the effective field theory approach at the LHC, J. High Energy Phys. 02 (2017) 115.
[41] R. Franceschini, G. Panico, A. Pomarol, F. Riva, and A. Wulzer, Electroweak precision tests in high-energy Diboson processes, J. High Energy Phys. 02 (2018) 111.
[42] G. F. Giudice, C. Grojean, A. Pomarol, and R. Rattazzi, The strongly-interacting light Higgs, J. High Energy Phys. 06 (2007) 045.
[43] R. Contino, A. Falkowski, F. Goertz, C. Grojean, and F. Riva, On the validity of the effective field theory approach to SM precision tests, J. High Energy Phys. 07 (2016) 144.
[44] M. Aaboud *et al.* (ATLAS Collaboration), Measurement of $W^{\pm}Z$ production cross sections and gauge boson polarisation in pp collisions at $\sqrt{s} = 13$ TeV with the ATLAS detector, Eur. Phys. J. C **79**, 535 (2019).
[45] Z. Bern *et al.*, Left-handed W Bosons at the LHC, Phys. Rev. D **84**, 034008 (2011).
[46] G. Panico, F. Riva, and A. Wulzer, Diboson interference resurrection, Phys. Lett. B **776**, 473 (2018).
[47] A. Azatov, J. Elias-Miro, Y. Reyimuaji, and E. Venturini, Novel measurements of anomalous triple gauge couplings for the LHC, J. High Energy Phys. 10 (2017) 027.
[48] G. Aad *et al.* (ATLAS Collaboration), Measurement of total and differential W^+W^- production cross sections in proton-proton collisions at $\sqrt{s} = 8$ TeV with the ATLAS detector and limits on anomalous triple-gauge-boson couplings, J. High Energy Phys. 09 (**2016**) 029.
[49] V. Khachatryan *et al.* (CMS Collaboration), Measurement of the W^+W^- cross section in pp collisions at $\sqrt{s} = 8$ TeV and limits on anomalous gauge couplings, Eur. Phys. J. C **76**, 401 (2016).
[50] M. Aaboud *et al.* (ATLAS Collaboration), Measurement of the W^+W^- production cross section in pp collisions at a centre-of-mass energy of $\sqrt{s} = 13$ TeV with the ATLAS experiment, Phys. Lett. B **773**, 354 (2017).
[51] M. Aaboud *et al.* (ATLAS Collaboration), Measurement of fiducial and differential W^+W^- production cross-sections at $\sqrt{s} = 13$ TeV with the ATLAS detector, Eur. Phys. J. C **79**, 884 (2019).
[52] G. Aad *et al.* (ATLAS Collaboration), Measurements of $W^{\pm}Z$ production cross sections in pp collisions at $\sqrt{s} =$ 8 TeV with the ATLAS detector and limits on anomalous gauge boson self-couplings, Phys. Rev. D **93**, 092004 (2016).
[53] V. Khachatryan *et al.* (CMS Collaboration), Measurement of the WZ production cross section in pp collisions at $\sqrt{s} = 7$ and 8 TeV and search for anomalous triple gauge couplings at $\sqrt{s} = 8$ TeV, Eur. Phys. J. C **77**, 236 (2017).
[54] A. M. Sirunyan *et al.* (CMS Collaboration), Measurements of the $pp \to WZ$ inclusive and differential production cross section and constraints on charged anomalous triple gauge couplings at $\sqrt{s} = 13$ TeV, J. High Energy Phys. 04 (2019) 122.
[55] A. Butter, O. J. P. Eboli, J. Gonzalez-Fraile, M. C. Gonzalez-Garcia, T. Plehn, and M. Rauch, The Gauge-Higgs legacy of the LHC Run I, J. High Energy Phys. 07 (2016) 152.
[56] M. Farina, G. Panico, D. Pappadopulo, J. T. Ruderman, R. Torre, and A. Wulzer, Energy helps accuracy: Electroweak precision tests at hadron colliders, Phys. Lett. B **772**, 210 (2017).
[57] J. Brehmer, S. Dawson, S. Homiller, F. Kling, and T. Plehn, Benchmarking simplified template cross sections in WH production, J. High Energy Phys. 11 (2019) 034.